Jan Stelzner* and Thorsten M. Buzug

Magnetic-field measurement and simulation of a field-free line magnetic-particle scanner

Abstract: In 2005, B. Gleich and J. Weizenecker initially presented the tracer based medical imaging modality Magnetic Particle Imaging (MPI). It uses the nonlinear magnetization behavior of super paramagnetic iron oxide nanoparticles (SPIONs). MPI has the potential to perform real-time imaging in the sub millimeter-range without the use of harmful radiation. To acquire a particle signal from the tracer, an alternating homogenous magnetic field (drive field) is applied. Due to the nonlinearity of the particle magnetization, the magnetic field is distorted and higher harmonics are generated that indicate a particle concentration within the field of view (FOV). For the spatial distribution, another magnetic field that exhibits a high gradient (selection field) is applied simultaneously. Basically, there are two different types of selection fields containing either a field-free point (FFP) or a field-free line (FFL). Because of magnetic saturation, only SPIONs within the close vicinity of the FFP or FFL contribute to the particle signal. As the FFP is moved by the drive field through the FOV a spatial distribution of the SPIONs can be obtained. In the other encoding concept, the FFL rotates and is additionally translated by the drive field to obtain one dimensional projections for various angles. In this work, the currently world's largest FFL MPI Scanner is investigated. Single components of the generated magnetic field are measured precisely to accomplish an accurate simulation of a translating and rotating FFL.

Keywords: MPI, Field-Free Line, Medical Imaging, Magnetic-Field Measurement, Field Simulation

https://doi.org/10.1515/cdbme-2017-0191

***Corresponding author: Jan Stelzner:** Institute for Medical Engineering, University of Lübeck, Ratzeburger Allee 160, 23562 Lübeck, Germany, e-mail: stelzner@imt.uni-luebeck.de
Thorsten M. Buzug: Institute for Medical Engineering, University of Lübeck, Ratzeburger Allee 160, 23562 Lübeck, Germany, e-mail: stelzner@imt.uni-luebeck.de

1 Introduction

As several foregoing works have shown, the properties of super paramagnetic substance can be used to record and investigate specific frequency spectra (MPS) [1,2]. The Langevin theory of paramagnetism describes the magnetization $\boldsymbol{M}$ as a function of the magnetic field strength $\boldsymbol{H}$ by the formula

$$\boldsymbol{M}(\boldsymbol{H}) = M_S \cdot L\left(\frac{\mu_0 m}{k_B T}\boldsymbol{H}\right), \qquad (1)$$

where M_S is the saturation magnetization, and L the Langevin function with the magnetic-field constant μ_0, the magnetic moment m and the thermal energy $k_B T$.
Applying a time varying sinusoidal magnetic field onto the SPIONs with an amplitude in the order M_S/μ_0 will cause a spectral finger print, where higher harmonics can be extracted to identify a magnetic-particle concentration within the generated field (see **Figure 1**).

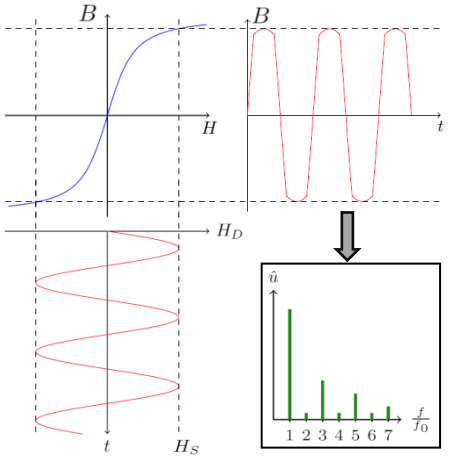

Figure 1: The basic principle of magnetic particle spectroscopy (MPS) and MPI. Applying an excitation field H_D with the fundamental frequency f_0 causes a modulation of the magnetic flux density $B(t)$ by the SPIONs. The receive signal u, which is proportional to the time derivative of $B(t)$ then contains higher harmonics.

Aiming for multidimensional imaging, a spatial encoding concept needs to be introduced. Therefore, an additional field, the selection field, is generated (see **Figure 2**).

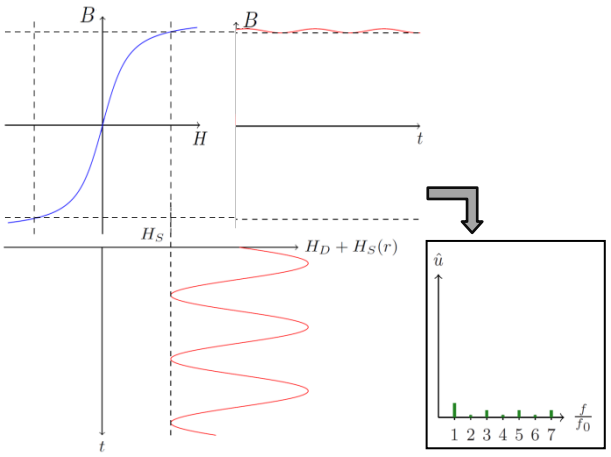

Figure 2: For spatial encoding, a selection field H_S is added, that shifts all SPIONs within the measurement field that are not in the close vicinity of the FFP or the FFL into magnetic saturation. Those particles do not respond to the drive field H_D.

1.1 Field-free line imaging

While first approaches and experiments were using a selection field containing an FFP, in 2008, a new concept of spatial encoding was published by Weizenecker et al. [3] where an FFL has been generated.

Due to the small magnitude of higher harmonics of the particle signal, the decisive advantage of an FFL is a higher signal-to-noise ratio (SNR) at equal bore size and gradient strength. As a drawback, while a selection field which yields an FFP only requires a coil pair in Maxwell configuration the necessary coil topology to generate and move an FFL fully electronically [4] is more complex and energy consuming. A reasonable setup for an FFL imaging-device contains two electromagnetic quadrupoles each one consisting of two orthogonally arranged Maxwell coil-pairs and furthermore, another Maxwell coil-pair aligned along the bore axis. For the drive field, two orthogonally arranged coil pairs in Helmholtz configuration are required to translate the FFL for every angle of the rotating FFL perpendicular to the bore axis (see **Figure 3**). The drive field currents carry the excitation frequency f_0 modulated with the rotational frequency of the FFL f_{rot}.

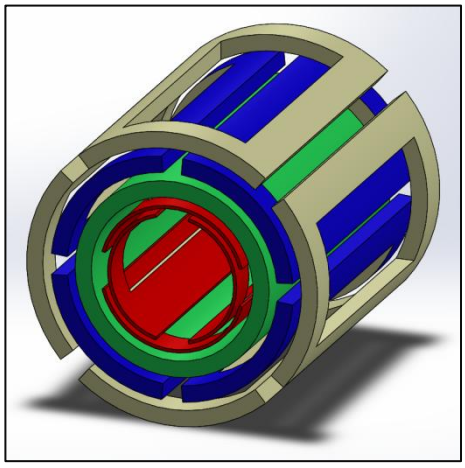

Figure 3: Coil topology of an electronically rotatable FFL Imaging-device. The red part represents the drive field coils for horizontal and vertical FFL translation, the green part the axial-gradient coil, the blue and the yellow part the quadrupoles.

2 Materials and methods

2.1 Setup of the investigated device

The setup of the investigated FFL imaging-device [5] corresponds to the concept described in section 1.1. The parameters of the imager are listed in **Table 1**.

Table 1: Parameters of the rabbit-sized MPI-FFL Scanner

Property	Value
Bore diameter	180 mm
Target gradient strength	0.8 T/m
Target drive field amplitude	15 mT
Target FFL-rotation frequency	10 Hz
Drive-field frequency	25 kHz
Drive-field generator cooling	Oil
Selection-field generator cooling	Water

To prevent high electric losses caused by the skin effect, the drive-field coils are made of high-frequency litz-wire. The power supply is provided by commercially available MRI amplifiers for the drive field generator and the quadrupoles and high-power direct-current (DC) sources for the axial-gradient coil.

2.2 Measurement of the selection field

As the axial gradient coil is fed by DC and the quadrupoles will be driven at a low frequency of f_s = 10 Hz the field measurements in this work were performed under quite similar conditions.

For these measurements, each field generating element was engaged at a time providing a constant magnetic field, which has been measured by a multi-axis hall probe. This probe was mounted onto a robot and placed into the center of the bore (see **Figure 4**). Then, a pattern perpendicular to the bore axis was scanned recording the Cartesian components of the magnetic flux-density B_x, B_y and B_z.

Figure 4: Setup of the selection-field measurement. A multi-axis hall-probe is mounted on a robot arm and records the magnetic flux density at various positions inside the bore.

These measurements were recorded inside a shielding room. The applied DC for the selection-field measurements amounted to 20 A. The expected field of each quadrupole exhibits an FFL in the center along the bore axis while the axial-gradient coil should feature an FFP, a steep gradient aligned with the bore axis and half of that gradient strength in radial direction.

2.3 Measurement of the drive field

For the measurement of the drive field a dedicated pick-up coil was constructed to reliably determine the magnetic flux density at the target frequency of f_0 = 25 kHz. The design was aiming for an induced voltage of exactly U_{ind} = 1 V per B = 1 mT at f_0. For a convenient size and feasibility the number of windings was set to N = 10. Following Faraday's law of induction, the cross section was calculated by eq. 2.

$$A = \frac{U_{\text{ind}}}{N \cdot 2\pi f_0 \cdot B} = 637\ \text{mm}^2 \qquad (2)$$

Using a circular cross section led to the radius for the pickup coils of r = 14.24 mm. Three coils of this kind were arranged perpendicular to each other to determine B_x, B_y and B_z. The construction process is depicted in **Figure 5**.

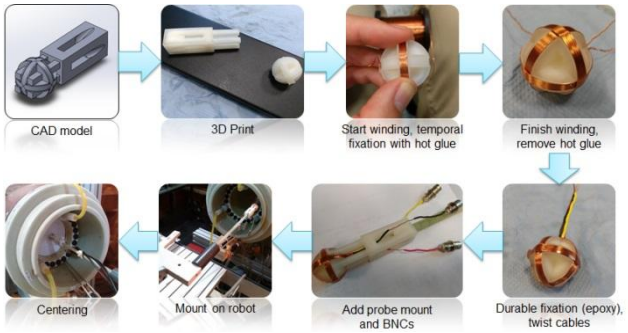

Figure 5: The process of the probe construction for the drive-field measurement. A mount head and a winding shape where printed by a photo-polymer 3D-printer, afterwards a 0.4 mm enamelled copper wire was wound around the shape and sealed with epoxy resin. After attaching BNCs, the probe was mounted onto the robot and driven into the measurement field.

For each measurement, the magnetic flux density was recorded at 17 different points. One in the center of the bore, 8 points in a distance of 3 cm and another 8 points 6 cm from the axial center. Then, those values are used for linear interpolation to acquire an appropriate field representation.

As the drive field generator is designed to provide a highly homogeneous magnetic field, the expected results show a similar amount of magnetic flux density for each measurement point without a significant change of the field direction.

3 Results

In this section, the magnetic-field measurements of the single elements of the coil topology the rabbit-sized MPI-FFL scanner involves are presented. In the first subsection, the magnetic-field components of the selection-field coils are shown, in the second one the field of the drive-field coils and in the third section, those partial fields are linearly combined to a rotatable, translatable FFL.

3.1 Selection-field measurement-results

Figure 6 shows the results of one of the quadrupoles. With a current of 20 A, the magnetic field features a gradient strength of approximately 10 mT/m.

Because the measurement slice is located near the center of the bore the axial component B_{axial} of the magnetic field is

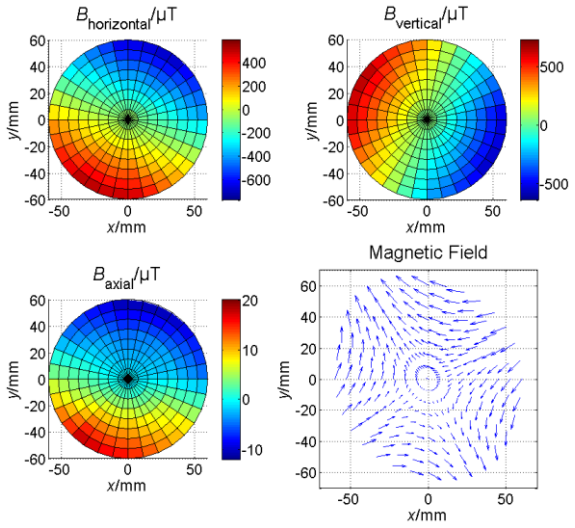

Figure 6: Interpolated magnetic flux density based on the Measurement in section 2.2. The top row shows the radial field components $B_{horizontal}$ and $B_{vertical}$, the bottom row the axial field component B_{axial} and the field direction and relative magnitude.

very low while the radial components $B_{horizontal}$ and $B_{vertical}$ change their field direction in orthogonal alignment to the bore axis and pass a value of zero near the center. The second quadrupole acts similarly with the whole field rotated by 45 degrees around the bore axis.

3.2 Drive-fields measurement-results

Figure 7 shows the results of the drive-field coil for the FFL translation in horizontal direction. The plots show that the horizontal field component is dominant and by about 2 orders of magnitude higher than the axial and the vertical field component. The quiver plot illustrates this behaviour.

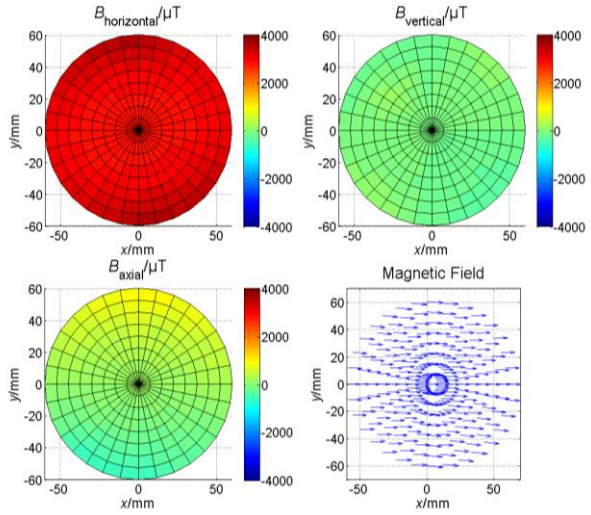

Figure 7: Interpolated magnetic flux density of the horizontal drive-field coil on a slice at the center of the bore.

3.3 Simulation of the FFL

To illustrate the capability of the setup to generate, rotate and translate an FFL, a linear combination of single field components is calculated and shown in **Figure 8** and **9**.

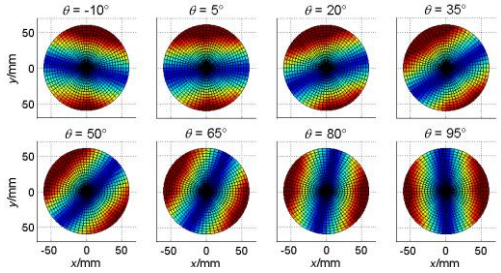

Figure 8: Simulation of the rotating FFL based on the measurements presented in section 3.1

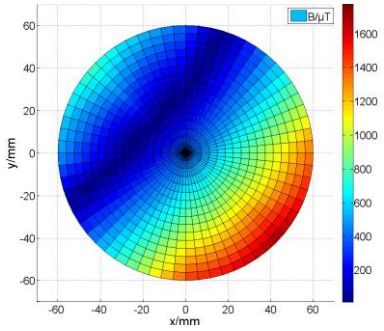

Figure 9: Rotated and translated FFL. In this simulated point in time, the FFL is rotated by 45° and translated by 15 mm.

Author's Statement

Research funding: The authors state no funding involved. Conflict of interest: Authors state no conflict of interest. Informed consent: Informed consent is not applicable. Ethical approval: The conducted research is not related to either human or animals use.

References

[1] B. Gleich and J. Weizenecker: Tomographic imaging using the nonlinear response of magnetic particles, Nature, 435, pp. 1214-1217, 2005, DOI:10.1038/nature03808

[2] S. Biederer et al.: Magnetization response spectroscopy of superparamagnetic nanoparticles for magnetic particle imaging, Journal of Physics D: Applied Physics, 42(20), 205007, 2009, DOI: 10.1088/0022-3727/42/20/205007

[3] J. Weizenecker, B. Gleich and J. Borgert: Magnetic particle imaging using a field free line. Journal of Physics D: Applied Physics, 41(10), 105009, 2008, DOI: 10.1088/0022-3727/41/10/105009

[4] K. Bente, M. Weber et al.: Electronic field free line rotation and relaxation deconvolution in magnetic particle imaging. IEEE Transactions on Medical Imaging, 34(2), pp. 644-651, 2014, DOI: 10.1109/TMI.2014.2364891

[5] G. Bringout et al: Concept of a Rabbit-Sized FFL-Scanner. 5th International Workshop on Magnetic Particle Imaging, p. 49, 2015, DOI: 10.1109/IWMPI.2015.7107